# Reliability Investigation of W2W Hybrid Bonding Interface: Breakdown Voltage and Leakage Mechanism


Lin Hou
*Western Digital*
Milpitas, CA 95035-7933, USA
Lin.Hou@wdc.com

Emmanuel Chery
*IMEC*
Leuven, Belgium
Emmanuel.Chery@imec.be

Kristof Croes
*IMEC*
Leuven, Belgium
Kristof.Croes@imec.be

Davide Tierno
*IMEC*
Leuven, Belgium
Davide.Tierno@imec.be

Soon Aik Chew
*IMEC*
Leuven, Belgium
Soon.Aik.Chew@imec.be

Yangyin Chen
*Western Digital*
Leuven, Belgium
Yangyin.Chen@wdc.com

Peter Rakbin
*Western Digital*
Milpitas, CA 95035-7933, USA
Peter.Rakbin@wdc.com

Eric Beyne
*IMEC*
Leuven, Belgium
Eric.Beyne@imec.be



***Abstract*—The electrical reliability of 1 µm pitch wafer-to-wafer (W2W) Cu/SiCN hybrid bonding interface is evaluated. Breakdown voltage distributions of the W2W hybrid stack were acquired using the controlled-IV method. Assuming a power law model, extrapolation towards use conditions confirm a lifetime above 10 years, with a power law exponent above 10 for temperatures under 175 °C. The conduction mechanism along the Cu/SiCN hybrid bonding interface is found to be Poole-Frenkel emission with energy barrier equals 0.95 eV. Mobile copper could only be observed at temperatures above 200 °C and for fields above 1.5 MV/cm, confirming the good robustness against copper drift for this bonding interface.**



***Index Terms*—Wafer-To-Wafer (W2W) bonding, reliability, dielectric breakdown, hybrid pad leakage.**


## I. Introduction

Wafer-to-wafer (W2W) hybrid bonding, which allows 3D stacking of chips by means of a hybrid-bonding interface, has recently attracted attention [1]–[4]. In W2W hybrid bonding technologies, two wafers are bonded together through copper damascene pads embedded in a dielectric material (i.e. $SiO_2$, SiCN) [3]. Several previous studies indicate that SiCN as bonding dielectric material shows higher bonding energy (2.4 J/m$^2$ after annealing at 250 °C for 2 hours) than $SiO_2$ (2.0 J/m$^2$) under the same bonding and thermal annealing conditions [3] [4]. SiCN also has been confirmed to be a good barrier material against copper diffusion [5]. While numerous studies have been conducted to improve the interfacial bonding strength and increase the interconnection density [2]–[4], the electrical properties and reliability of SiCN as a bonding dielectric have barely been investigated.

In this work, the Cu/SiCN hybrid bonding interface electrical reliability is studied using the controlled IV methodology [6] [7]. In addition, the conduction mechanism along with the bonding interface and its blocking properties against copper diffusion will be discussed.

## II. Test Vehicle and Structures

The W2W hybrid bonding scheme used in this work is shown in Fig. 1 (a). To improve the bonding alignment tolerance, the dimension of the bottom copper pad is designed to be larger than the top copper pad. The top and bottom pad diameter is 200 and 600 nm, respectively, with a pitch of 1 µm resulting in a critical pad to pad distance of 400 nm. The bottom pad width along the bonding interface is measured to be 680 nm by TEM cross-section as shown in Fig. 1 (b). For the 1 µm pad structure, the critical pad to pad spacing along the bonding is further corrected to be 320 nm. A thin layer of SiCN is capped on top of the $SiO_2$ layer. The thickness of the SiCN cap layer after CMP is measured to be 98 nm from the TEM image.

The top view and cross-sectional view of the TDDB structures on the designed test vehicle are shown in Fig. 2 (a) and (b), respectively. Each TDDB structure includes 250 fork-fork pairs, and each fork pair includes 90 pad pairs, resulting in a total of 22500 pad pairs for each test structure. As shown in Fig. 2 (b), two configurations are evaluated in this work: full pad structure and bottom half structure. The top metal and top pad are excluded for the bottom half structure. Other parameters, such as pad dimension, spacing, and pad number, remain identical in both configurations.

## III. Results and Discussion

### A. Breakdown Voltage Distributions and Controlled IV Methodology

The power law exponent $\gamma$, so-called field acceleration factor, is a key parameter which quantifies dielectric reliability. A high $\gamma$ gives an indication of high reliability under a certain operating field and vice versa [8]. An estimation of the field acceleration factor $\gamma$ can be obtained by measuring

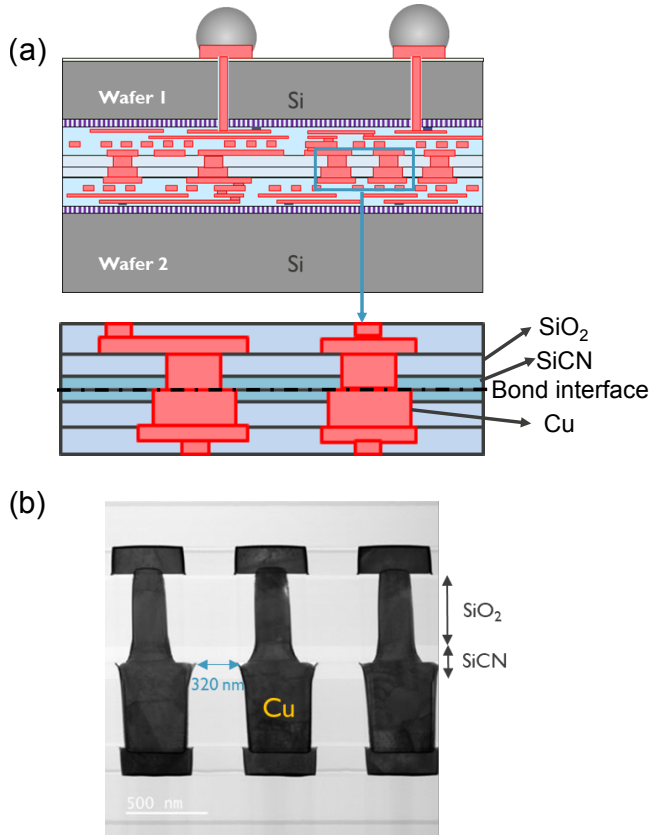


Fig. 1. (a) Schematic of W2W hybrid bonding; (b) TEM image in the daisy chain region. The critical pad spacing at the bonding interface is 320 nm.

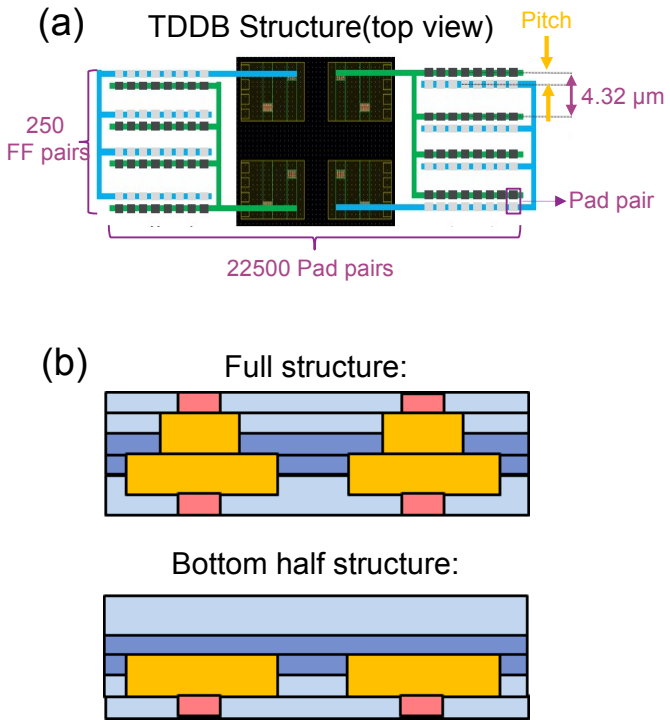


Fig. 2. Designed TDDB structures to evaluate the pad-to-pad breakdown and conduction mechanism (a)top view; (b)cross-section view

the breakdown voltage of the dielectric using several voltage ramp-up rates as already reported in the literature [6] [9].

The breakdown voltage along the bonding interface was evaluated for temperatures ranging from 100 to 200 °C using the controlled IV methodology. Three different ramp rates (1.15 V/s, 0.26 V/s and 0.06 V/s) were applied to the two different pad configurations to record the current change versus voltage. An example of current vs. voltage (200 °C) for our hybrid pad structure is shown in Fig. 3. The dielectric breakdown happens at around 114 V, resulting in a significant increase of leakage current. As shown in Fig. 1 (b), the bonding interface has the shortest distance between pad pairs, resulting in the maximum local electrical field along the bonding interface. As a consequence, the breakdown of the pad pair is likely happening along the bonding interface.

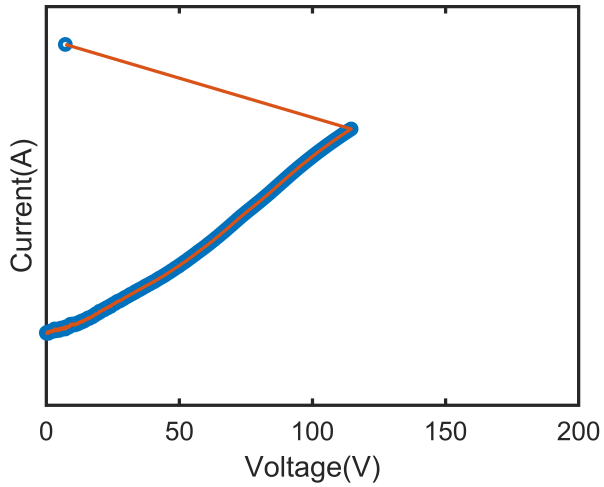


Fig. 3. An example of current vs. voltage for full pad structure dielectric breakdown. Dielectric breakdown happens at 114 V and leakage current increases significantly afterwards.

The Weibull plots of breakdown voltage ($V_{BD}$) distributions for the full pad configuration as a function of the ramp rate at different temperatures are shown in Fig. 4. The $V_{BD}$ values for hybrid pad with 320 nm spacing are much higher than 100 V below 200 °C. As expected, $V_{BD}$ depends on the ramp rate. The voltage ramp rate affects the $V_{BD}$ since the voltage increments take time to induce TDDB stress effects. Therefore, the measurement with a lower ramp-up shows a lower $V_{BD}$. The time-to-failure (TTF) 63 % values for various ramp rates could be extracted based on the Weibull probability plots. The extracted TTF 63 % values were further used to extract field the acceleration factor $\gamma$. Besides the dependancy on the ramp rate, dielectric breakdown is affected by temperature. As shown in the cumulative distribution plots of full pad structure from Fig. 4 , a strong decrease in the breakdown voltage and Weibull slope is observed when the temperature reaches 200 °C. No strong decrease trend could be observed up to 175 °C.

The power-law field acceleration factor, $\gamma$ , can be extracted by plotting the ramp rate as a function of the breakdown voltage. The estimated field acceleration factors at various

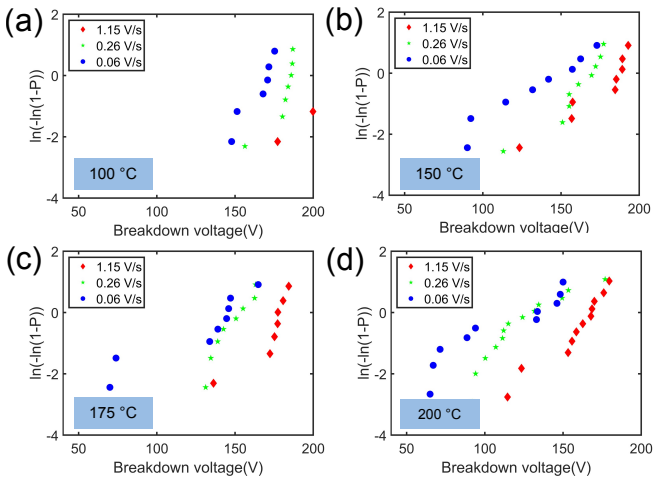


Fig. 4. Weibull plot of breakdown voltage distribution for full pad structures measured by controlled-IV method (a) 100 °C; (b) 150 °C; (c) 175 °C; (d) 200 °C.

temperatures for the full pad structures are shown in Fig. 5. $\gamma$ is in a range of 11-13 when the temperature is below 200 °C. At 200 °C, we observed a decrease of $\gamma$. Assuming a Power-law model [9] [10], the extrapolated lifetime (for mean time to failure) at use condition is estimated to be well above 10 years, resulting in a $V_{max}$ around 27 V at 100 °C for the test structure with 22500 pad pairs. The $V_{max}$ of full pad structure at 200 °C decreases to 11.4 V due to a lower field acceleration factor $\gamma$. The reduction of $\gamma$ observed at 200 °C could be linked to copper drift in the SiCN layer. This will be further discussed later in this work.

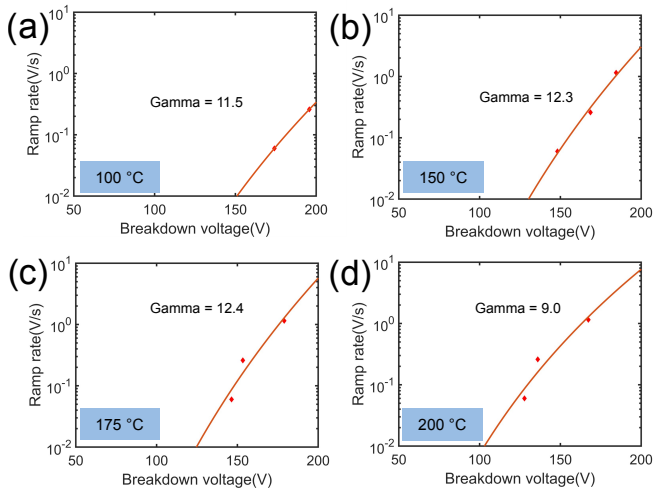


Fig. 5. Field acceleration factor $\gamma$ for full pad structures based on $V_{BD}$ under (a) 100 °C; (b) 150 °C; (c) 175 °C; (d) 200 °C.

The Weibull plots of breakdown voltage ($V_{BD}$) distributions for the bottom half pad configuration as a function of the ramp rate and the corresponded field acceleration factor $\gamma$ at different temperatures (100, 150 and 200 °C) are shown in Fig. 6. Similar trends could be observed on the bottom half

TABLE I
THE EXTRACTED ACCELERATION FACTORS $\gamma$ AND $V_{max}$ (ABOVE 10 YEARS LIFETIME) FOR FULL STRUCTURE AND BOTTOM HALF STRUCTURE (CRITICAL SPACING EQUALS 320 NM )

| Temperature(°C) | Full structure | | Bottom half structure | |
|---|---|---|---|---|
| | $\gamma$ | Vmax (V) | $\gamma$ | Vmax (V) |
| 100 | 11.5 ± 0.1 | 26.9 ± 0.4 | 12.6 ± 0.1 | 30.0 ± 0.4 |
| 150 | 12.3 ± 0.2 | 27.4 ± 0.8 | 15.8 ± 0.1 | 40.6 ± 0.4 |
| 175 | 12.4 ± 0.4 | 25.3 ± 1.3 | - | - |
| 200 | 9.0 ± 0.4 | 11.4 ± 1.2 | 7.5 ± 0.1 | 9.7 ± 0.4 |

TDDB pad configuration. The measured $V_{BD}$ values are also much higher than 100 V below 200 °C. A decrease of $V_{BD}$ and Weibull slope could be observed at 200 °C (Fig. 6 (c)). Similarly, the reduction of $\gamma$ results in a relatively low $V_{max}$ value (9.7 V) at 200 °C compared to 100 and 150 °C.

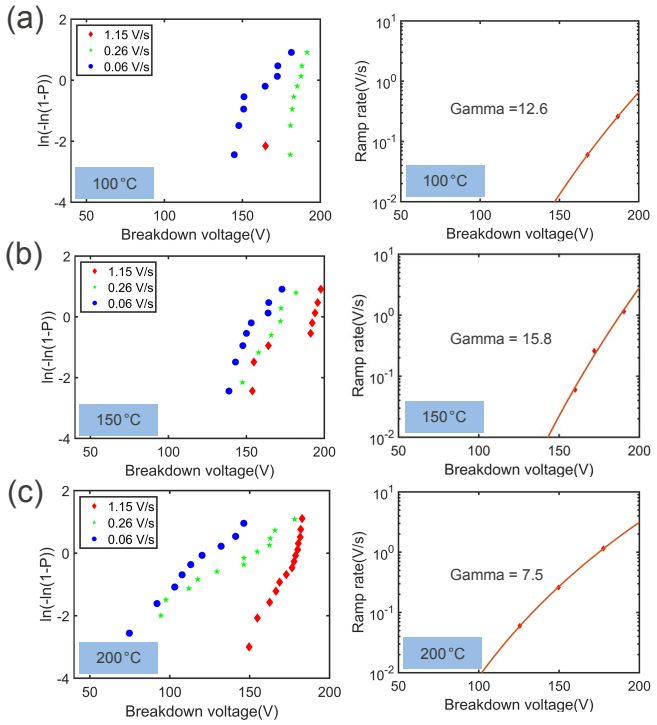


Fig. 6. Weibull plot of breakdown voltage distribution and corresponded acceleration factor $\gamma$ of bottom half structures measured by controlled-IV method (a) 100 °C; (b) 150 °C; (c) 200 °C

The obtained acceleration factors and $V_{max}$ for the two TDDB pad configurations are listed in Table I. The similar trends between the full structure and the bottom half structure indicate a limited impact of top metal/pad on interfacial breakdown since the existence of top metal/pad does not influence the critical spacing between pad pairs.

### *B. Conduction Mechanism*

Conduction mechanisms describe how electrons travel from one electrode to the other electrode. It provides a relationship between the leakage currents and the electric fields applied

to the material. Different conduction mechanisms have been reported for FEOL gate oxide and BEOL barrier/dielectrics [11]–[14]. Schottky emission (SE) and Poole-Frenkel (PF) describe field-enhanced thermal excitation of electrons conducting from interfaces and trap states of dielectric, respectively. The relationships between current density vs. electrical field for SE and PF emission are given as follows:

$$J_{PF} \sim Eexp[\frac{-q(\varphi_{PF} - \sqrt{\frac{qE}{\pi\varepsilon_0 k}})}{k_B T}] \quad (1)$$

$$J_{SE} \sim T^2 exp[\frac{-q(\varphi_{SE} - \sqrt{\frac{qE}{4\pi\varepsilon_0 k}})}{k_B T}] \quad (2)$$

where $J$ is current density, $k_B$ is Boltzmann constant, $T$ is temperature, $q$ is the elementary charge, $\varphi$ is barrier height (trap depth), $E$ is electric field, $k$ is dielectric constant, $\varepsilon_0$ is permittivity of free space.

To investigate the dominant conduction mechanisms along the bonding interface, current-voltage sweeps were performed for temperatures ranging from 25 to 300 °C. The leakage current density vs. electrical field of the full pad structure is shown in Fig.7. The extracted dielectric constants ($>$ 1 MV/cm) using Poole-Frenkel and Schottky emission equations in the temperature range 25 to 300 °C are listed in Table II. As shown in the table, the extracted dielectric constant based on PF emission falls within a range of 4.6 to 6.3. Those values are very close to the dielectric constant (k = 4.9) of a bulk SiCN layer. The extracted dielectric constants based on SE are all around 1. Such kind of observation is not realistic for W2W hybrid bonding test structures since k = 1 typically indicates a structure with the air gap. It also implies that the leakage current is mainly located in the SiCN bonding interface rather than in the bulk $SiO_2$ layer (k = 3.9 for $SiO_2$). Therefore, the conduction mechanism in the SiCN dielectric layer is found to follow Poole-Frenkel emission when the electrical field is higher than 1 MV/cm.

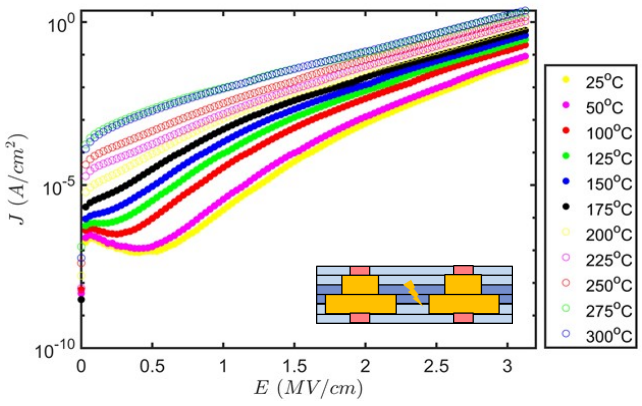


Fig. 7. Current density vs. electrical field with the temperature range of 25-300 °C for full pad structure(center die).

TABLE II
THE EXTRACTED PERMITTIVITY (DIELECTRIC CONSTANT) BASED ON POOLE-FRENKEL EMISSION AND SCHOTTKY EMISSION.

| Temperature(°C) | PF emission | Schottky emission |
|---|---|---|
| 25 | 4.8 | 1.2 |
| 50 | 4.6 | 1.1 |
| 100 | 4.9 | 1.2 |
| 125 | 5.1 | 1.3 |
| 150 | 5.2 | 1.3 |
| 175 | 5.3 | 1.3 |
| 200 | 5.4 | 1.4 |
| 225 | 4.8 | 1.2 |
| 250 | 5.0 | 1.3 |
| 275 | 6.3 | 1.5 |
| 300 | 5.4 | 1.4 |

By re-plotting ln(J/E) as a function of $\sqrt{E}$ (Fig.8 (a)), the activation energy of the leakage current as a function of the electrical field assuming a PF conduction mechanism is extracted, as shown in Fig.8 (b). The equations for the two plots in Fig.8 are shown as follows:

$$ln(\frac{J_{PF}}{E}) \sim \frac{-q(\varphi_{PF} - \sqrt{\frac{qE}{\pi\varepsilon_0 k}})}{k_B T} \quad (3)$$

with

$$Ea = q(\varphi_{PF} - \sqrt{\frac{qE}{\pi\varepsilon_0 k}}) \quad (4)$$

The intercept of Ea vs. $\sqrt{E}$ curve in the linear regions is used to extract the barrier height/trap depth $\varphi$ for PF emission and the barrier height (trap depth) was found to be around 0.95 eV. This value is close to the trap depth value reported for SiCN layers in the BEOL copper damascene process [15].

### C. Cu Drift

Plots of current density vs. temperature (-1/kT) for the full pad structure at 1.5 MV/cm and 2.5 MV/cm are shown in Fig. 9 (a) and (b), respectively. It can be seen from the plots that current density versus temperature shows a simple linear relationship from 25 to 300 °C at 1.5 MV/cm. For a relatively high electric field, i.e., 2.5 MV/cm, a transition point of current density vs. temperature could be seen at 200 °C. When temperature $>$ 200 °C, the observed increased leakage current density (indicated by black dot line) suggests that there is a different dominant mechanism besides Poole-Frenkel emission. Such kind of observation is in good agreement with our previous observation of the decrease of Weibull slope and $V_{BD}$ values at 200 °C by controlled-IV methodology.

Since the increase of leakage current density could only be observed at high temperature ($>$ 200 °C) and high electrical field ($>$ 1.5 MV/cm), one potential hypothesis is that copper starts to drift under these stress conditions. This hypothesis is further verified by applying a constant current stress (I = 300 µA) at 200 °C on the full pad structure and bottom half structure [16]. Plots of voltage (V) versus time (s) for full pad structure and bottom half structure are shown in Fig. 10 (a) and

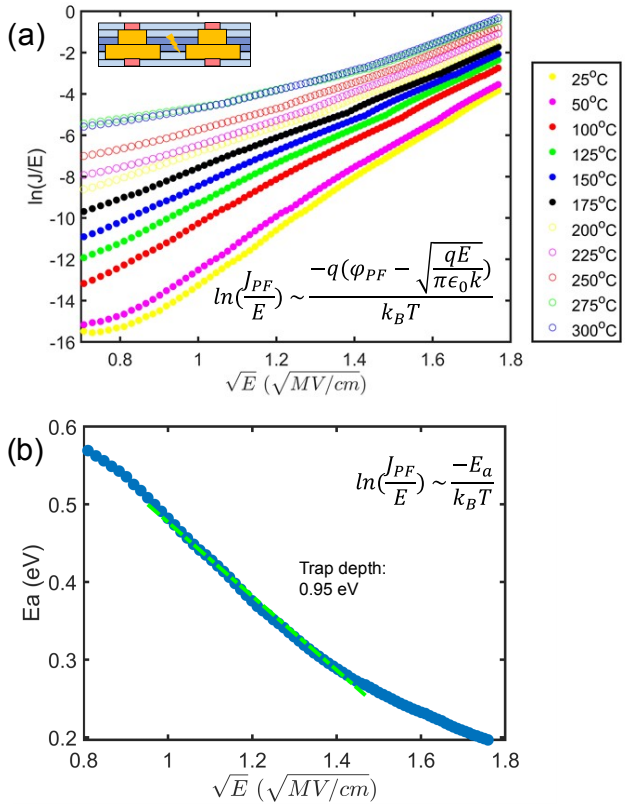


Fig. 8. The activation energy (Poole-Frenkel emission) vs. electrical field for full pad structure. Trap depth $\varphi$ could be extracted from the linear fitting of Ea vs. $\sqrt{E}$

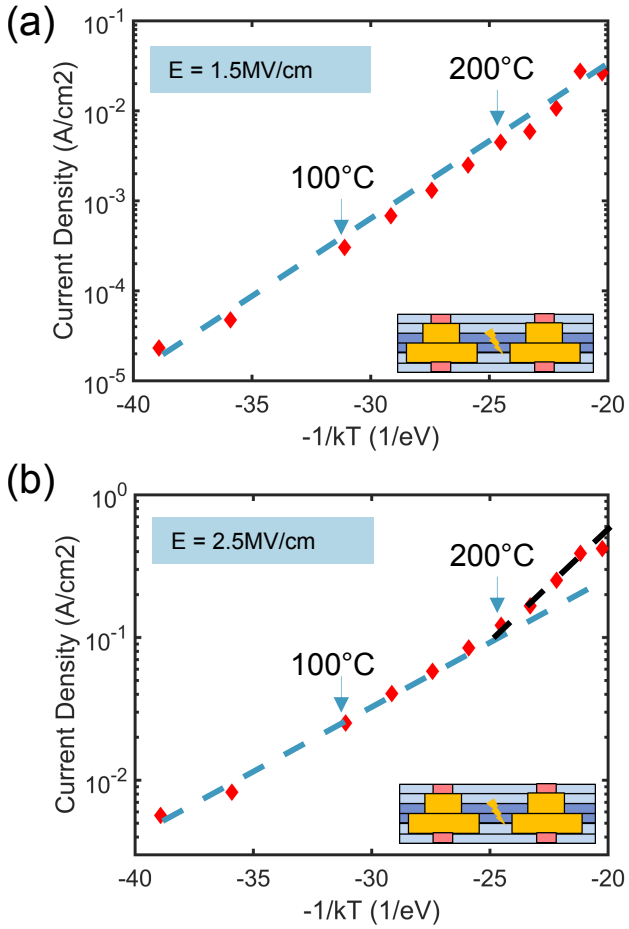


Fig. 9. Current density vs.-1/kT under (a) low electrical field (1.5 MV/cm); (b) high electrical field (2.5 MV/cm)

(b), respectively. The equivalent electrical fields (calculated from the measured voltages) are also indicated. As shown in the plots, both structures present a soft breakdown behavior when facing a constant current stress. After a few hundred seconds, a sharp decrease of the voltage is observed, but the voltage does not reach 0 V. This behavior is the signature of a soft breakdown behavior resulting from the formation of a copper filament.

Previous studies [17]–[19] indicate that SiCN shows a higher resistance to copper drift compared to $SiO_2$. Copper drift in $SiO_2$ could occur at a relatively low electrical field (1 MV/cm) and low temperature (100/150 °C), based on the studies of Loke et al. [17] and Shacham-Diamand et al. [18]. Those observed threshold values of electric field and temperature are much lower compared to our current observations for SiCN as a dielectric barrier for copper drift. Zhao et al. [19] also reported that clear evidence of copper contamination in $SiO_2$ on PCAP structure that field acceleration factor is drastically decreased when positively stressed in $SiO_2$. Such effect was not observed in the same PCAP structure with SiCN as the dielectric layer.

Note that copper thermal diffusion is also present but much less critical for both $SiO_2$ and SiCN. The study of Shacham-Diamand et al. [18] indicates that a copper concentration of $10^{17}$ $cm^{-3}$ can be reached by copper diffusion while 1000 times higher concentrations ($10^{21}$ $cm^{-3}$) are obtained in presence of a field. Overall, SiCN was demonstrated to be a good barrier material to prevent copper diffusion by several investigations [20] [21].

## IV. Conclusions

W2W Cu/SiCN hybrid bonding interface electrical reliability was evaluated in this work. $V_{BD}$ distributions under various temperatures/V-ramp rates were acquired using the controlled IV methodology. Power law acceleration factors measured on several pad configurations were found to be in the range of 11-16 for temperatures below 200 °C. Assuming a power-law model, the extrapolated lifetime at use condition exceeds 10 years. A decrease of $V_{BD}$ values and Weibull slope could be observed when the temperature reaches 200 °C.

The conduction mechanism along the Cu/SiCN hybrid bonding interface was characterized and found to follow Poole-Frenkel emission. An increased leakage current is only observed at 200 °C and for fields above 1.5 MV/cm. These results are in good agreement with the decrease of $V_{BD}$ values and Weibull slopes observed at 200 °C and were further linked to copper drift in the dielectric by constant current stress.

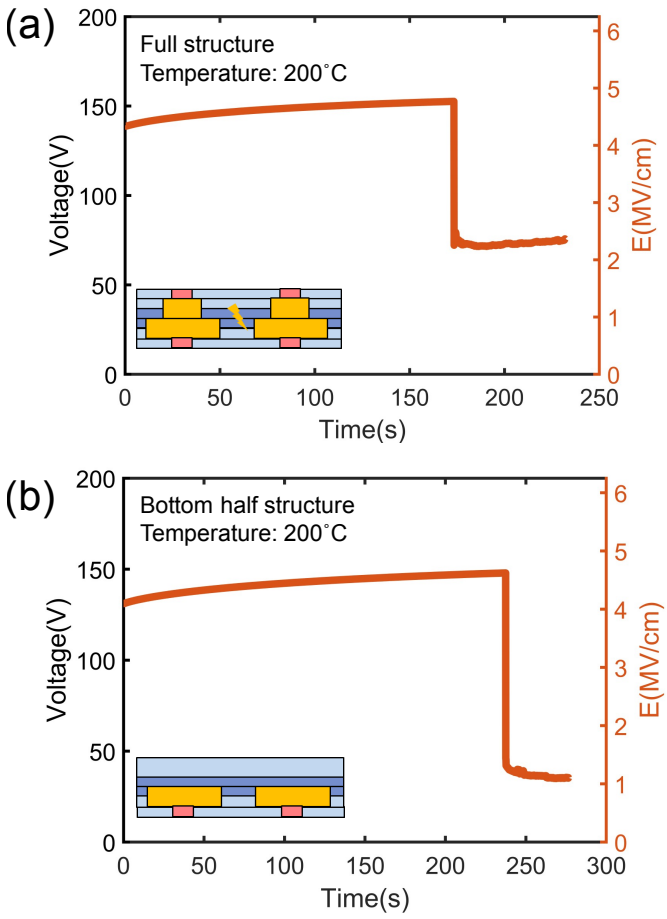


Fig. 10. Constant current stress(I= 300 µA) on (a) full pad structure at 200 °C; (b) bottom half structure at 200 °C.

Since the degradation of reliability and increase of leakage current only happens when the temperature reaches 200 °C and for electrical field above 1.5 MV/cm, copper drift is not currently considered as a concern below 200 °C for the studied hybrid bonding scheme. To conclude, our investigations indicate a robust W2W hybrid bonding process using SiCN as bonding dielectric material.

## ACKNOWLEDGMENT

The authors gratefully acknowledge the contributions from IMEC 3D team for hybrid bonding wafer process. We are also thankful to M. Stucchi for discussions.

## REFERENCES

[1] Utsumi, Jun, Kensuke Ide, and Yuko Ichiyanagi. "Cu/$SiO_2$ hybrid bonding obtained by surface-activated bonding method at room temperature using Si ultrathin films." Micro and Nano Engineering 2 (2019): 1-6.

[2] Beyne, Eric, et al. "Scalable, sub 2 µm pitch, Cu/SiCN to Cu/SiCN hybrid wafer-to-wafer bonding technology." 2017 IEEE International Electron Devices Meeting (IEDM). IEEE, 2017.

[3] Peng, Lan, et al. "Advances in sicn-sicn bonding with high accuracy wafer-to-wafer (w2w) stacking technology." 2018 IEEE International Interconnect Technology Conference (IITC). IEEE, 2018.

[4] Kim et. al, Method of bonding semiconductor substrates 2018, US10141284B2.

[5] K. Goto, H. Yuasa, A. Andatsu and M. Matsuura, "Film characterization of Cu diffusion barrier dielectrics for 90 nm and 65 nm technology node Cu interconnects." Proceedings of the IEEE 2003 International Interconnect Technology Conference (Cat. No. 03TH8695). IEEE, 2003.

[6] Berman, Arnold. "Time-zero dielectric reliability test by a ramp method." 19th International Reliability Physics Symposium. IEEE, 1981.

[7] Li, Yunlong, et al. "Electrical characterization method to study barrier integrity in 3D through-silicon vias." 2012 IEEE 62nd Electronic Components and Technology Conference. IEEE, 2012.

[8] Li, Yunlong, et al. "Impact of barrier integrity on liner reliability in 3D through silicon vias." 2013 IEEE International Reliability Physics Symposium (IRPS). IEEE, 2013

[9] Aal, A. "TDDB Data Generation for Fast lifetime Projections Based on V-Ramp Stress Data" IEEE Transactions on Device and Materials Reliability, 2007, 7, 278-284

[10] Croes, Kristof, et al. "Current understanding of BEOL TDDB lifetime models." ECS Journal of Solid State Science and Technology 4.1 (2014): N3094.

[11] Ohring, Milton. Reliability and failure of electronic materials and devices. Elsevier, 1998

[12] Colinge, J-P., & Cynthia A. Colinge. Physics of semiconductor devices. Springer Science & Business Media, 2005.

[13] Vilmay, M.; Roy, D.; Volpi, F. & Chaix, J. M. "Characterization of low-k SiOCH dielectric for 45nm technology and link between the dominant leakage path and the breakdown localization" Microelectronic Engineering, 2008, 85, 2075-2078.

[14] K. -. Allers, R. Schwab, W. Walter, M. Schrenk and H. Korner, "Thermal and dielectric breakdown for metal insulator metal capacitors (MIMCAP) with tantalum pentoxide dielectric," IEEE International Integrated Reliability Workshop Final Report, 2002., 2002, pp. 96-101.

[15] Guedj, C., et al. "Dielectric Conduction Mechanisms of Advanced Interconnects: Evidence for Thermally-Induced 3D/2 D Transition." 2006 IEEE International Reliability Physics Symposium Proceedings. IEEE, 2006.

[16] Ciofi, I., Mannarino, M., Li, Y., Croes, K., & Beyer, G. P. (2012). "Self-Controlled Constant-Current Temperature Stress for Triangular Voltage Sweep Measurements of Cu." ECS Transactions, 41(43), 113.

[17] Loke, Alvin LS, et al. "Kinetics of copper drift in PECVD dielectrics." IEEE Electron device letters 17.12 (1996): 549-551.

[18] Shacham-Diamand, Y., et al. "Copper transport in thermal SiO2." Journal of the Electrochemical Society 140.8 (1993): 2427.

[19] Zhao, Larry, et al. "A novel test structure to study intrinsic reliability of barrier/low-k." 2009 IEEE International Reliability Physics Symposium. IEEE, 2009.

[20] Zhou, Ji-Cheng, Zhi-Jie Shi, and Xu-Qiang Zheng. "Preparation and properties of SiCN diffusion barrier layer for Cu interconnect in ULSI." Transactions of Nonferrous Metals Society of China 19.3 (2009): 611-615.

[21] Prasad, K., et al. "Evaluation of diffusion barrier layers in Cu interconnects." 2002 Conference on Optoelectronic and Microelectronic Materials and Devices. COMMAD 2002. Proceedings (Cat. No. 02EX601). IEEE, 2002.